Editors' Suggestion | Featured in Physics

Gardening on the Moon: An Advection-Diffusion Model to Guide the Search for Supernova Debris in the Lunar Regolith

Emily S. Costello*
Hawaii Institute of Geophysics and Planetology, University of Hawaii at Mānoa, Honolulu, Hawaii 96822, USA

John Ellis
Theoretical Particle Physics and Cosmology Group, Department of Physics, King's College London, London WC2R 2LS, United Kingdom and Theoretical Physics Department, CERN, CH-1211 Geneva 23, Switzerland

Brian D. Fields
Departments of Astronomy and of Physics, and Illinois Center for the Advanced Study of the Universe, University of Illinois, Urbana, Illinois 61801, USA

Rebecca Surman
Department of Physics and Astronomy, University of Notre Dame, Notre Dame, Indiana 46556, USA

Xilu Wang
State Key Laboratory of Particle Astrophysics, Institute of High Energy Physics, Chinese Academy of Sciences, Beijing 100049, China

(Received 18 April 2026; revised 8 June 2026; accepted 12 June 2026; published 14 August 2026)

The vertical redistribution of materials in the lunar regolith—ranging from continuously produced space-weathering products to sporadic pulses of supernova- or kilonova-derived isotopes—remains a fundamental problem in planetary science. We present a unified stochastic model of regolith gardening induced by the impact flux. Treating gardening as a competition between impact-driven advection and diffusion predicts the maturity profiles of *Apollo* cores over more than 2 orders of magnitude in time (1.4×10^7 to 4.5×10^8 yr). This model describes well the depth profiles of live ^{60}Fe in *Apollo* regolith samples, suggesting that supernova dust capture is independent of native iron abundance, and is consistent with a uniform influx at the latitudes of the *Apollo* landing sites. We extend our model to predict lunar signals for live *r*-process species that might originate from supernovae or kilonovae: ^{244}Pu tied to terrestrial detections, and ^{129}I, ^{182}Hf, and ^{247}Cm based on *r*-process calculations. The ^{244}Pu/^{60}Fe depth profile can probe the origin of ^{244}Pu, motivating searches in *Artemis* regolith samples down to depths $\mathcal{O}(100)$ cm.

DOI: 10.1103/14kh-nkgl

Introduction—The lunar regolith serves as a record-keeper of the Solar System's history, preserving evidence of solar wind, cosmic rays, and episodic interstellar events. However, this record is scrambled by impact gardening. Gardening is a stochastic vertical transport process driven by the flux of crater-forming impacts over 12 orders of magnitude in scale [1,2]. Classically, the cumulative effects of gardening are treated as a diffusive "random walk" (see, e.g., Ref. [3]). However, high-resolution depth profiles of regolith maturity (the optical and physical changes that result from exposure to space) and isotopic tracers consistently exhibit sharp gradients and vertical centroids that are mathematically incompatible with purely diffusive smearing (see, e.g., Ref. [4]).

Models for regolith gardening are crucial for studying the infall of debris from nearby astrophysical events. It was suggested in [5] that nearby supernova explosions might have deposited on Earth small but detectable amounts of ^{60}Fe and other live isotopes such as ^{244}Pu (for a recent review see Ref. [6]). Deep-sea deposits of ^{60}Fe were subsequently reported by [7] and many subsequent experiments, and ^{60}Fe has also been found in *Apollo* samples of the lunar regolith [8]. Subsequently, ^{244}Pu has also been discovered in deep-ocean [9–11] and terrestrial [12] deposits. The terrestrial ^{60}Fe was mainly deposited in a pulse about 2.3 million years ago (Mya) [13], with a smaller, earlier pulse about 7.3 Mya [11]. These pulses could be due either to shock fronts passing through the Solar System or

*Contact author: costello@higp.hawaii.edu

Published by the American Physical Society under the terms of the Creative Commons Attribution 4.0 International license. Further distribution of this work must maintain attribution to the author(s) and the published article's title, journal citation, and DOI.

to the Earth passing through overdensities in the local interstellar medium due to clouds or walls of the bubble blown by prior supernova explosions. ^{60}Fe is also seen in cosmic rays [14], further indicating that nearby supernovae were recently present and powered particle acceleration [15–17].

^{244}Pu has also been detected in deep-sea samples; the signal spans both ^{60}Fe pulses, but the earlier time structure is unclear [11]. This has provoked discussion [18] of whether or not the ^{60}Fe and ^{244}Pu have a common origin. The ^{60}Fe signal originates in a core-collapse supernova; other sources such as asymptotic giant branch stars underproduce ^{60}Fe or cannot deliver it to Earth [19]. ^{244}Pu is exclusively produced by the astrophysical *r* process, which may take place in exceptional supernovae or in kilonovae (collisions of neutron stars) [20], with the latter likely to produce ^{244}Pu more copiously, along with iodine and other elements that are essential for human life [21]. Given ^{244}Pu's longer half-life ($t_{1/2} = 81.3$ Myr) than ^{60}Fe [$t_{1/2} = 2.60(5)$ Myr], older deposits may remain detectable. Their time structure, alongside other *r*-process isotopes like ^{129}I, ^{182}Hf, and ^{247}Cm [18], could illuminate their origin.

Conversely, supernova-produced ^{60}Fe may serve as a critical new probe of vertical transport mechanisms in the regolith. Isotopic analysis of *Apollo* 11, 12, 15, and 16 samples revealed ^{60}Fe activities exceeding cosmic-ray production by a factor $\mathcal{O}(30)$ [8,22]. While this signal likely records supernova debris deposition ∼2 Mya, the present depth profile convolves the initial deposition flux with subsequent mechanical gardening.

Gardening model—Lunar impacts redistribute regolith by excavating, compacting, and burying material. We present a mass-conservative analytic model of this transport efficiency, updating previous frameworks [1,2,23,24]. Defining depth z (positive downward from the surface at $z = 0$) and exposure time t, the net vertical transport depth $D_z(t)$ is the sum of downward drivers (burial, compaction) minus the upward driver (exhumation),

$$D_z(t) = D_B(t) + D_C(t) - D_E(t) = \underbrace{\left[\eta_b(b) + \frac{h_c}{c_c^{-\frac{2}{b-2}}} - \frac{h_e}{c_e^{-\frac{2}{b-2}}}\right]}_{\text{Geometric Efficiency}} \underbrace{\left(\frac{\pi a b t}{4(b-2)\lambda}\right)^{\frac{1}{b-2}}}_{\text{Probabilistic Frequency}}, \quad (1)$$

where $\eta_b(b)$ is the effective burial efficiency (defined as a summation over ejecta annuli), h_c and h_e are the vertical reach scales for compaction and excavation, c_c and c_e are their respective horizontal interaction scales, and a, b, and λ characterize the impact production function and frequency [see Supplemental Material (SM) [25] Sec. S1 for full derivations and parameter values].

Differentiating Eq. (1) yields the vertical transport velocity $v_z(t)$ (derived in SM Sec. S2 [25]). For the steep secondary impactor slopes ($b \approx 4$) adopted here, $v_z > 0$, driving a net downward advection of surface materials, whereas shallower primary slopes drive upward exhumation.

Stochastic vertical mixing by smaller craters above this advective front is captured by a diffusion coefficient $\kappa(t)$, defined by the variance of impact-driven displacements relative to the transient crater reach (detailed in SM Sec. S2 [25]).

This kinematic model allows the regolith to be treated as a continuum where the evolution of a concentration or number density $C(z,t)$ is governed by the following advection-diffusion equation (ADE):

$$\frac{\partial C}{\partial t} = \frac{\partial}{\partial z}\left(\kappa(t)\frac{\partial C}{\partial z}\right) - v_z(t)\frac{\partial C}{\partial z} - \lambda_{\text{decay}} C + S(z,t), \quad (2)$$

where $S(z,t)$ represents the spatiotemporal source term (continuous for maturity, episodic for supernova-derived ^{60}Fe, and continuous or depth-dependent for cosmogenic ^{60}Fe) and $\lambda_{\text{decay}} = 1/\tau$ is the radioactive decay rate given the mean life τ. When solving this equation, we treat the surface as a flux boundary.

Results—

Validation (Regolith maturity): Incorporating secondary impacts as the primary vertical transport driver [24], our model reproduces characteristic I_s/FeO profiles across *Apollo* 15, 16, and 17 cores, whose ages are independently constrained by cosmic ray tracks and radionuclide benchmarks [4,34] (Fig. 1). This correspondence across 2 orders of magnitude in exposure age (∼1.4×10^7 to 4.5×10^8 yr) suggests the maturation front directly manifests the advective-diffusive equilibrium established by the impact size-frequency distribution. The I_s/FeO agreement for ^{60}Fe-analyzed *Apollo* 15 and 16 cores validates the modeled gardening history over tens to hundreds of millions of years—ancient enough to reach steady-state cosmogenic production (Fig. 1).

While the ADE solution captures bulk transport, the stochastic nature of individual impacts introduces concentration fluctuations, as observed in core data [4] (see Fig. 1). We utilize these residuals from the maturity validation to define a conservative site-agnostic empirical uncertainty envelope. By aggregating the normalized variance between our most-probable model lines and the observed I_s/FeO profiles, we derive a global standard deviation ($\sigma_{\text{global}} \approx 0.24$) that represents the inherent noise of the gardening process (SM Sec. S4 [25]). This envelope provides a statistically realistic benchmark for the forward-modeled distributions of episodic species such as ^{60}Fe and ^{244}Pu, accounting for the fact that any single core is a discrete realization of a locally unique impact history.

Episodic sources (Supernova ^{60}Fe): To evaluate incident interstellar debris, we introduce a spatiotemporal source term $S(z,t)$ driven by a surface flux $\Phi(t)$. For ^{60}Fe, deep-sea measurements indicate distinct

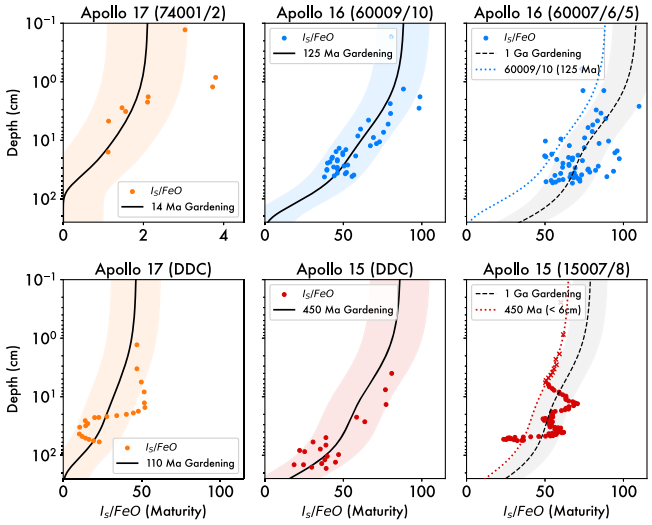


FIG. 1. Surface maturity profiles for *Apollo* 15, 16, and 17 samples that validate the unified gardening model. Observed I_s/FeO maturity indices [4] (colored points) are compared with gardening model results (black lines). For the four cores on the left, model timescales (t) are constrained by independent cosmic ray track and cosmogenic radionuclide densities reported in [4]; for the two cores on the right [8], a 1 Ga reference mixing profile and the gardening profile of the dated core from the same landing region are shown (black dashed and colored dotted lines, respectively). Shaded bands represent the empirical error ($\sigma = 0.24$). The model translates time-integrated gardening flux $\mathcal{M}(z,t)$ into maturity by accounting for the depth-dependent bulk density $\rho(z)$ (1.3–1.9 g/cm^3; see SM Sec. S3 [25]), such that $I_s/\mathrm{FeO}(z) \propto \mathcal{M}(z,t)/\rho(z)$. In order to account for mineralogy-dependent variations in space-weathering efficiency and initial iron abundance between landing sites, model profiles are fluence-matched to the observed data.

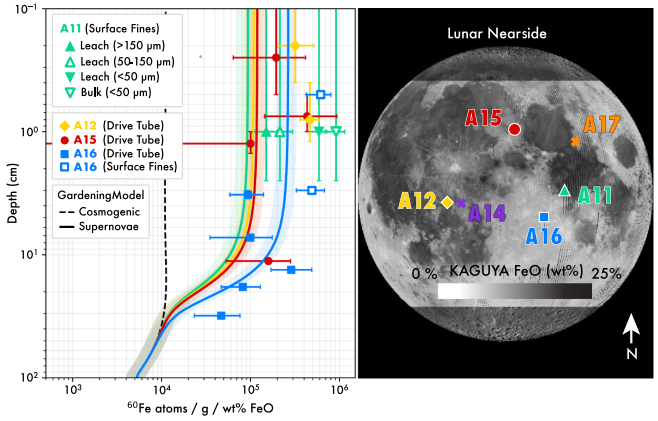


FIG. 2. Left: depth profile of ^{60}Fe across *Apollo* landing sites. ADE model results for the combination of two known supernova pulse events are shown as colored solid lines scaled for specific *Apollo* sites, compared with lunar soil data from [8] and [22]. To isolate the supernova-source signal, measured activities are converted to atoms per unit mass, normalized by the stable Ni concentration and, importantly, normalized by the average FeO wt% of the respective landing site (as detailed in SM Sec. S3.4 [25]). A11 data [22] separate bulk dissolved fractions from leached fractions across varying grain sizes. Horizontal error bars represent the propagation of 1σ measurement uncertainties. The shaded bands around the model contours denote the model uncertainty ($\sigma = 0.24$) propagated from the validated gardening parameters in Fig. 1. The dashed black line represents the modeled steady-state *in situ* cosmogenic background floor. Right: nearside of the Moon, with locations of the *Apollo* landing sites shown and a Kaguya Multiband Imager FeO wt% map overlay [27].

supernova-originated pulses. We model this flux as a superposition of Gaussian pulses parametrized by their fluence, restricting deposition to the surface (SM Sec. S3.2 [25]).

As discussed in SM [25], data on deep-ocean deposits of ^{60}Fe provide evidence of two pulses: a stronger pulse that reached Earth ~3 Mya and a weaker pulse that arrived ~7 Mya. It is plausible that there were earlier nearby supernovae [35,36], but the data on deep-ocean deposits do not extend beyond ~10 Mya and, in view of the short half-life of ^{60}Fe, any earlier ^{60}Fe pulse seems unlikely to remain detectable.

The pulse parameters from SM Table II [25] include the Earth's interstellar ^{60}Fe fluence that corrects marine crust measurements for a 17% uptake efficiency, determined by comparing the ^{60}Fe flux into the crust with the flux into deep-sea sediments [11]. We conservatively assume an isotropic radioisotope flux, motivated by the "pinball" model of magnetically confined dust grains [37]. Assuming a single direction would increase the inferred interstellar flux fourfold by correcting the Earth's surface-area to cross-section ratio.

The left panel of Fig. 2 compares lunar measurements in *Apollo* 11, 12, 15, and 16 samples of the excess ^{60}Fe (after subtraction of the cosmic-ray contribution) with the prediction of the ADE model with the two known ^{60}Fe pulses (lines with uncertainty shaded). We see that, despite having the different native iron contents [26,27] shown in the right panel of Fig. 2, the *Apollo* 15 and 16 core samples show similar ^{60}Fe inventories that are consistent with the ADE model predictions. This agreement boosts confidence in the ADE gardening model, and also shows that the adopted ^{60}Fe flux is consistent with the lunar data. This agreement suggests that the radioisotope flux may be closer to isotropic than unidirectional.

The finest fraction (< 50 μm) of mature surface regolith from Apollo 11 (A11) [22], and samples of the upper few centimeters of soil from A16 and the A12 drive tube [8], exhibit higher ^{60}Fe concentrations than predicted by models of cosmogenic production, supernova delivery, and impact gardening (Fig. 2). This anomaly suggests that the smallest, most mature size fractions of lunar soil are exceptionally efficient at capturing exogenic ^{60}Fe while simultaneously suppressing the cosmogenic background. This dual effect is likely governed by space weathering, as discussed in SM S5 [25].

As noted in [38], if supernova debris containing ^{60}Fe retains directional information until reaching the Solar System, the dependence of ^{60}Fe deposition density on lunar latitude could constrain the source direction. The difference in latitude between the *Apollo* 15 and 16 landing sites (see the right panel of Fig. 2) provides a limited lever arm, and it is not surprising that the *Apollo* 15 and 16 samples have similar ^{60}Fe inventories. *Artemis* measurements of the ^{60}Fe inventory at the lunar South Pole could provide valuable insight, though directional information may have been lost during propagation if the ^{60}Fe-carrying dust grains were deflected by interstellar magnetic fields [13,37].

Forward modeling (^{244}Pu and other *r*-process species) To evaluate long-term *r*-process isotope sequestration, we forward-model concentration profiles of ^{244}Pu ($t_{1/2} = 81.3$ Myr) and coproduced species. Unlike ^{60}Fe, ^{244}Pu's long half-life permits tracking interstellar influx and gardening dynamics over 100 Myr timescales. Using the ADE model [Eq. (2)] on a 0 to 80 cm spatial grid, we simulate three astrophysical histories to test if vertical distributions can distinguish episodic from steady-state ^{244}Pu delivery (Fig. 3).

For the *r*-process species, we use the observed deep-sea ratio $(^{244}\mathrm{Pu}/^{60}\mathrm{Fe})_{\mathrm{deep-sea}} = (4.7 \pm 5) \times 10^{-5}$ [11] to infer the ^{244}Pu flux from the ^{60}Fe flux during the last 9 Myr when these have been measured. To illustrate the result for other *r*-process radioisotopes, we adopt the kilonova-inspired "KA" model in [18] to give production ratios to ^{244}Pu. The abundance ratios of ^{129}I, ^{182}Hf, and ^{247}Cm relative to ^{244}Pu for H1 and H2 are taken from Table 1 of [18] and Table 5 of [39], respectively. Adopted *r*-process quantities appear in Table II in SM [25].

We consider three flux histories to illustrate widely different but possible *r*-process deposition on Earth. We use the resulting $\Phi(t)$ in the source term (SM Sec. S3.2 [25]) and defined the following histories.

History 1 (H1): Correlation with supernova pulses (solid line): ^{244}Pu and *r*-process delivery is fully coupled to the two recent supernova events (2.3 and 7.3 Mya) identified in the ^{60}Fe record, with the same Gaussian peak times and widths. For each pulse the ^{244}Pu fluence is derived from the ^{60}Fe fluence: $\mathcal{F}_{244} = (^{244}\mathrm{Pu}/^{60}\mathrm{Fe})_{\mathrm{deep-sea}}\mathcal{F}_{60}$. Because the deposition is relatively recent, the signal is primarily sequestered in the upper 10 cm, showing sharp gradients.

History 2 (H2): Short-term continuous influx (dashed line): A constant source flux of $\Phi = 250 \times 10^{-6}$ atoms/cm^2 is applied over the last 10 Myr. This models a steady-state accumulation of interstellar dust during the Solar System's recent passage through local debris clouds. The profile exhibits a morphology similar to the solar maturity (I_s/FeO).

History 3 (H3): Long-term continuous influx (dotted line): The same constant ^{244}Pu flux is applied over 80 Myr. Over this longer duration, the advective front

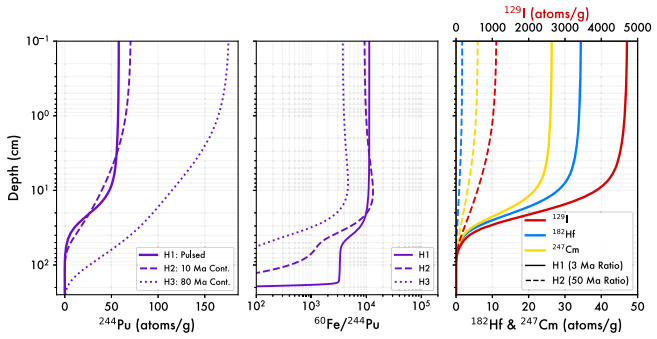


FIG. 3. Left: forward modeled ^{244}Pu depth profiles in various delivery histories. The model is applied to pulsed delivery (H1; solid), short-term continuous accumulation (H2, 10 Myr; dashed), and long-term saturation (H3, 80 Myr; dotted). Profiles are normalized by density (SM S6 [25]). Depth-resolved ^{244}Pu profiles clearly distinguish between recent astrophysical events and a longer downpour of interstellar dust but give no hints as to whether the ^{244}Pu and ^{60}Fe sources are the same or distinct. Center: ratio of ^{60}Fe and ^{244}Pu abundances as a function of depth in histories H1, H2, H3 for ^{244}Pu production. We see that depth-resolved ^{244}Pu profiles can distinguish clearly between histories H1 and H2 and history H3. Right: depth-integrated *r*-process concentrations (^{129}I, top; ^{182}Hf, ^{247}Cm, bottom) following a pulsed delivery centered at 2.3 and 7.3 Mya for H1 (solid lines), and a continuous influx over the last 10 Myr for H2 (dashed lines) with an injection time of 50 Myr. The corresponding *r*-process isotope production ratios relative to ^{244}Pu are given in Tables 5 and 6 of [39]. Source terms are scaled to the ^{244}Pu global reference (2.21×10^3 atoms/g). The depth distributions reflect the competition between impact-driven gardening and radioactive decay. A linear-scaled version of this figure is provided in SM (Sec. S7) [25].

$v_z(t)$ and cumulative diffusion $\kappa(t)$ transport the isotope significantly deeper and more thoroughly into the column, and the integration of signal over a longer time period leads to a larger total fluence.

The difference between Histories 1 and 3 suggests that isotopic analysis of deep regolith samples (e.g., $z > 20$ cm) can serve as a diagnostic tool, as indicated in the left panel of Fig. 3. A deep-seated ^{244}Pu tail would imply a persistent interstellar background, whereas a signal restricted to the upper reworking zone would support an origin tied to recent, discrete supernova events. The global empirical error envelope ($\sigma_{\mathrm{global}} \approx 0.24$) indicates that these histories remain statistically resolvable despite the stochastic nature of impact gardening.

Histories 1 and 2 give similar results for ^{244}Pu. For these cases, therefore, distinguishing between possible origins of a persistent interstellar background, e.g., multiple supernovae or kilonovae, would require complementary diagnostic tools, e.g., measurements of the density profiles of other live isotopes such as ^{129}I ($t_{1/2} = 16.1$ Myr), ^{182}Hf ($t_{1/2} = 8.90$ Myr), or ^{247}Cm [$t_{1/2} = 15.6(5)$ Myr], as seen in the right panel of Fig. 3. In this panel, we consider an

r-process source that either is coincident with the iron pulses and plutonium production as in History 1 or is a separate, earlier event that is also responsible for the plutonium continuum influx in History 2. In the former, we take the r-process radioisotopes to be produced along with the pulses at 2.3 and 7 My at ratios consistent with the KA model of [39], while in the latter we take the r-process production to have occurred with the same ratios but at a much earlier time, which we take to be $t_{\rm inj} = 50$ Myr. This is meant to account for an earlier r-process event whose ejecta is later swept up in the local bubble—the hot, rarefied medium carved out by $\mathcal{O}(10)$ supernovae [40,41]. The production timescale is consistent with our earlier work [39], and similar to but somewhat smaller than the estimated neutron star merger recurrence time in [42]. The flux of r-process isotope i, which is $\Phi_{i,\rm inj}$, upon injection will decay so that later $\Phi_i(t) = \Phi_{i,\rm inj} e^{-\lambda_i(t_{\rm inj}-t)}$. Given the shorter half-lives of the other r-process radioisotopes, measurements of these species relative to ^{244}Pu can potentially distinguish between the two scenarios.

Forward modeling (prospective south polar isotope measurements): We anticipate that *Artemis* missions will be able to gather regolith core samples that supplement and complement the information gleaned from the *Apollo* samples. It will be interesting to compare measurements of the ^{60}Fe density profile near the South Pole with the *Apollo* measurements at mid-latitudes. If the direction to the ^{60}Fe source is retained during transport to the Solar System [38], the density of ^{60}Fe deposition will depend on lunar latitude, and the comparison of *Apollo* measurements with South Pole data will give indications on the location of the source of the ^{60}Fe. However, the directional information may have been lost during transport from the source, e.g., due to deflection of the dust grains carrying ^{60}Fe by interstellar magnetic fields [37], in which case the *Apollo* and *Artemis* measurements of ^{60}Fe should be similar.

As seen in the left panels of Figs. 2 and 3, it will be interesting to obtain regolith core samples extending to depths $\gtrsim$100 cm, which will probe the possible deposition of live isotopes over timescales longer than the half-life of ^{60}Fe. For example, the density profile of ^{244}Pu relative to ^{60}Fe may be enhanced dramatically at depth if its deposition has been occurring since before the two detected ^{60}Fe pulses.

Discussion—Our ADE model matches the ^{60}Fe depth profiles measured in *Apollo* samples. The uniform ^{60}Fe signal across nearside mid-latitudes suggests a capture mechanism decoupled from local mineralogy. We have applied our ADE model to predict the possible depth profile of ^{244}Pu in different deposition scenarios. If deposition of ^{244}Pu has been taking place continuously over the past 10×10^6 yr, it may be present in the lunar regolith down to a depth $\mathcal{O}(10)$ cm, whereas if deposition has been continuing for 80×10^6 yr or more its depth profile may extend to a depth $\mathcal{O}(100)$ cm. Thus, the lunar regolith may provide insights into the history of the Solar System extending far beyond the reach of $\sim 10 \times 10^6$ yr provided by deep-ocean deposits. As we have also discussed, searches for other live r-process isotopes such as ^{129}I, ^{182}Hf, and ^{247}Cm will also be informative. Planned regolith samples should be well-suited to our needs, but we urge that care be taken to avoid contamination that could spoil measurements of the radioisotopes of interest.

Future measurements of the ^{60}Fe signal and other live isotopes across different sampling depths and latitudes, including samples returned by *Chang'E-5* and *6* and other *Apollo* cores, may indicate possible source directions. South Polar regolith samples, to be collected by future missions including those of the *Artemis* program, will be particularly interesting in this regard, as they provide a larger latitudinal lever arm than the *Apollo* measurements.

Acknowledgments—We acknowledge digitized data from [4] and [8]. The work of E. S. C. was sponsored by the National Aeronautics and Space Administration's Lunar Reconnaissance Orbiter project under a contract to the University of California at Los Angeles, (Principal Investigator, David A. Paige) and a Cassini Data Analysis Program Grant (80NSSC25K7448). The work of J. E. was supported by the United Kingdom STFC Grant No. ST/X000753/1. The work of B. D. F. was supported by the NSF Grant No. AST-2108589. The work of X. W. was supported by the National Natural Science Foundation of China (Grants No. 12494570, No. 12494574, No. 12521005), the National Key R&D Program of China (2021YFA0718500), and China's Space Origins Exploration Program. The work of R. S. was supported by US Department of Energy Grants No. DE-FG0295ER40934 and No. DE-SC00268442 (ENAF) and NSF Awards No. PHY-2020275 (N3AS) and No. 21-16686 (NP3M).

Data availability—We acknowledge Apollo soil maturity data digitized data from Morris [4] and isotope abundance data digitized from Fimiani *et al.* [8], and Zwickel *et al.* [22]. The impact gardening model can be reproduced from equations provided in Supplemental Material [25].

[1] D. Gault, F. Hörz, D. Brownlee, and J. Hartung, Mixing of the lunar regolith, in *Lunar Science Conference, 5th, Houston, Texas, March 18–22, 1974, Proceedings* (Pergamon Press, Inc., New York, 1974), Vol. 3 and 5 (A75-39540 19-91), pp. 2365–2386.

[2] E. S. Costello, R. R. Ghent, and P. G. Lucey, The mixing of lunar regolith: Vital updates to a canonical model, Icarus **314**, 327 (2018).

[3] M. Siegler, R. Miller, J. Keane, M. Laneuville, D. Paige, I. Matsuyama, D. Lawrence, A. Crotts, and M. Poston, Lunar true polar wander inferred from polar hydrogen, Nature (London) **531**, 480 (2016).
[4] R. V. Morris, *In situ* reworking/gardening/of the lunar surface-evidence from the Apollo cores, in *Lunar and Planetary Science Conference, 9th, Houston, Texas, March 13–17, 1978, Proceedings* (Pergamon Press, Inc., New York, 1978), Vol. 2 and 9 (1978), pp. 1801–1811.
[5] J. R. Ellis, B. D. Fields, and D. N. Schramm, Geological isotope anomalies as signatures of nearby supernovae, Astrophys. J. **470**, 1227 (1996).
[6] B. D. Fields and A. Wallner, Deep-sea and lunar radioisotopes from nearby astrophysical explosions, Annu. Rev. Nucl. Part. Sci. **73**, 365 (2023).
[7] K. Knie, G. Korschinek, T. Faestermann, C. Wallner, J. Scholten, and W. Hillebrandt, Indication for supernova produced ^{60}Fe activity on earth, Phys. Rev. Lett. **83**, 18 (1999).
[8] L. Fimiani, D. L. Cook, T. Faestermann, J. M Gómez-Guzmán, K. Hain, G. Herzog, K. Knie, G. Korschinek, P. Ludwig, J. Park *et al.*, Interstellar ^{60}Fe on the surface of the moon, Phys. Rev. Lett. **116**, 151104 (2016).
[9] M. Paul, A. Valenta, I. Ahmad, D. Berkovits, C. Bordeanu, S. Ghelberg, Y. Hashimoto, A. Hershkowitz, S. Jiang, T. Nakanishi, and K. Sakamoto, Experimental limit to interstellar ^{244}Pu abundance, Astrophys. J. Lett. **558**, L133 (2001).
[10] C. Wallner, T. Faestermann, U. Gerstmann, K. Knie, G. Korschinek, C. Lierse, and G. Rugel, Supernova produced and anthropogenic ^{244}Pu in deep sea manganese encrustations, New Astron. Rev. **48**, 145 (2004).
[11] A. Wallner, M. B. Froehlich, M. A. C. Hotchkis, N. Kinoshita, M. Paul, M. Martschini, S. Pavetich, S. G. Tims, N. Kivel, D. Schumann, M. Honda, H. Matsuzaki, and T. Yamagata, ^{60}Fe and ^{244}Pu deposited on Earth constrain the *r*-process yields of recent nearby supernovae, Science **372**, 742 (2021).
[12] S. Bishop, I. Stanciu, A. Cabré, C. Feibel, D. Pacesila, A. Petre, P. Mereuta, L. Trache, M. Virgolici, C. Pintilie, A. Serban, A. Petraglia, F. Terrasi, F. Marzaioli, G. Porzio, R. Buompane, and L. Gialanella, Discovery of extraterrestrial ^{244}Pu in 2 million year old fossilized stromatolites, Planet. Sci. J. **6**, 75 (2025).
[13] A. F. Ertel, B. J. Fry, B. D. Fields, and J. Ellis, Supernova dust evolution probed by deep-sea ^{60}Fe time history, Astrophys. J. **947**, 58 (2023).
[14] W. R. Binns, M. H. Israel, E. R. Christian, A. C. Cummings, G. A. de Nolfo, K. A. Lave, R. A. Leske, R. A. Mewaldt, E. C. Stone, T. T. von Rosenvinge, and M. E. Wiedenbeck, Observation of the ^{60}Fe nucleosynthesis-clock isotope in galactic cosmic rays, Science **352**, 677 (2016).
[15] M. Kachelrieß, A. Neronov, and D. V. Semikoz, Cosmic ray signatures of a 2–3 Myr old local supernova, Phys. Rev. D **97**, 063011 (2018).
[16] D. Benyamin and N. J. Shaviv, Lower limits on the nucleosynthesis of ^{44}Ti and ^{60}Fe in the dynamic spiral-arm cosmic-ray propagation model, Astrophys. J. **863**, 86 (2018).
[17] C. Nojiri, N. Globus, and E. Ramirez-Ruiz, Life in the bubble: How a nearby supernova left ephemeral footprints on the cosmic-ray spectrum and indelible imprints on life, Astrophys. J. Lett. **979**, L18 (2025).
[18] X. Wang, A. M. Clark, J. Ellis, A. F. Ertel, B. D. Fields, B. J. Fry, Z. Liu, J. A. Miller, and R. Surman, Proposed lunar measurements of *r*-process radioisotopes to distinguish the origin of deep-sea ^{244}Pu, Astrophys. J. **948**, 113 (2023).
[19] B. J. Fry, B. D. Fields, and J. R. Ellis, Astrophysical shrapnel: Discriminating among near-earth stellar explosion sources of live radioactive isotopes, Astrophys. J. **800**, 71 (2015).
[20] B. P. Abbott *et al.* (LIGO Scientific, Virgo, Fermi GBM, INTEGRAL, IceCube, AstroSat Cadmium Zinc Telluride Imager Team, IPN, Insight-Hxmt, ANTARES, Swift, AGILE Team, 1M2H Team, Dark Energy Camera GW-EM, DES, DLT40, GRAWITA, Fermi-LAT, ATCA, ASKAP, Las Cumbres Observatory Group, OzGrav, DWF (Deeper Wider Faster Program), AST3, CAASTRO, VINROUGE, MASTER, J-GEM, GROWTH, JAGWAR, CaltechNRAO, TTU-NRAO, NuSTAR, Pan-STARRS, MAXI Team, TZAC Consortium, KU, Nordic Optical Telescope, ePESSTO, GROND, Texas Tech University, SALT Group, TOROS, BOOTES, MWA, CALET, IKI-GW Follow-up, H.E.S.S., LOFAR, LWA, HAWC, Pierre Auger, ALMA, Euro VLBI Team, Pi of Sky, Chandra Team at McGill University, DFN, ATLAS Telescopes, High Time Resolution Universe Survey, RIMAS, RATIR, SKA South Africa/MeerKAT Collaborations), Multi-messenger observations of a binary neutron star merger, Astrophys. J. Lett. **848**, L12 (2017).
[21] J. Ellis, B. D. Fields, and R. Surman, Do we owe our existence to gravitational waves?, Phys. Lett. B **858**, 139028 (2024).
[22] S. Zwickel, S. Fichter, D. Koll, M. Hotchkis, J. Lachner, M. Norman, S. Pavetich, G. Rugel, K. Stübner, S. Tims, and A. Wallner, Simultaneous extraction of cosmogenic and interstellar radionuclides from lunar soil, Nucl. Instrum. Methods Phys. Res., Sect. B **573**, 166008 (2026).
[23] E. S. Costello, R. R. Ghent, M. Hirabayashi, and P. G. Lucey, Impact gardening as a constraint on the age, source, and evolution of ice on Mercury and the Moon, J. Geophys. Res. **125**, e2019JE006172 (2020).
[24] E. S. Costello, R. R. Ghent, and P. G. Lucey, Secondary impact burial and excavation gardening on the Moon and the depth to ice in permanent shadow, J. Geophys. Res. **126**, e2021JE006933 (2021).
[25] See Supplemental Material at http://link.aps.org/supplemental/10.1103/14kh-nkgl for further details on the advection-diffusion gardening model and linear-scale depth distributions, which includes Refs. [26–33]. Aspects of our numerical analysis are described in Sec. S8 in SM.
[26] D. Trang and P. G. Lucey, Improved space weathering maps of the lunar surface through radiative transfer modeling of Kaguya multiband imager data, Icarus **321**, 307 (2019).
[27] M. Lemelin, P. G. Lucey, E. Song, and G. J. Taylor, Lunar central peak mineralogy and iron content using the Kaguya multiband imager: Reassessment of the compositional structure of the lunar crust, J. Geophys. Res. **120**, 869 (2015).

[28] P. Brown, R. Spalding, D. O. ReVelle, E. Tagliaferri, and S. Worden, The flux of small near-earth objects colliding with the Earth, Nature (London) **420**, 294 (2002).
[29] H. J. Melosh, *Impact Cratering: A Geologic Process* (Oxford University Press, New York; Clarendon Press, Oxford, 1989).
[30] N. N. D. Center, Nudat database, https://www.nndc.bnl.gov/nudat/, accessed: 2026-04-02.
[31] D. Koll, A 10-million year time profile of interstellar influx to Earth mapped through supernova ^{60}Fe and *r*-process ^{244}Pu, Ph.D. thesis, Australian National University, 2023.
[32] A. R. Vasavada, J. L. Bandfield, B. T. Greenhagen, P. O. Hayne, M. A. Siegler, J.-P. Williams, and D. A. Paige, Lunar equatorial surface temperatures and regolith properties from the diviner lunar radiometer experiment, J. Geophys. Res. **117**, E00H18 (2012).
[33] P. O. Hayne, J. L. Bandfield, M. A. Siegler, A. R. Vasavada, R. R. Ghent, J.-P. Williams, B. T. Greenhagen, O. Aharonson, C. M. Elder, P. G. Lucey *et al.*, Global regolith thermophysical properties of the moon from the diviner lunar radiometer experiment, J. Geophys. Res. **122**, 2371 (2017).
[34] G. Heiken, D. Vaniman, and B. M. French, *Lunar Sourcebook: A User's Guide to the Moon* (Cup Archive, Cambridge, UK, 1991).
[35] D. Breitschwerdt, J. Feige, M. Schulreich, M. d. Avillez, C. Dettbarn, and B. Fuchs, The locations of recent supernovae near the Sun from modelling ^{60}Fe transport, Nature (London) **532**, 73 (2016).
[36] M. M. Schulreich, J. Feige, and D. Breitschwerdt, Numerical studies on the link between radioisotopic signatures on Earth and the formation of the local bubble. II. Advanced modelling of interstellar ^{26}Al, ^{53}Mn, ^{60}Fe, and ^{244}Pu influxes as traces of past supernova activity in the solar neighbourhood, Astron. Astrophys. **680**, A39 (2023).
[37] B. J. Fry, B. D. Fields, and J. R. Ellis, Magnetic imprisonment of dusty pinballs by a supernova remnant, Astrophys. J. **894**, 109 (2020).
[38] B. J. Fry, B. D. Fields, and J. R. Ellis, Radioactive iron rain: Transporting ^{60}Fe in supernova dust to the ocean floor, Astrophys. J. **827**, 48 (2016).
[39] X. Wang, A. M. Clark, J. Ellis, A. F. Ertel, B. D. Fields, B. J. Fry, Z. Liu, J. A. Miller, and R. Surman, *r*-process radioisotopes from near-Earth supernovae and kilonovae, Astrophys. J. **923**, 219 (2021).
[40] P. C. Frisch, S. Redfield, and J. D. Slavin, The interstellar medium surrounding the sun, Annu. Rev. Astron. Astrophys. **49**, 237 (2011).
[41] C. Zucker, A. A. Goodman, J. Alves, S. Bialy, M. Foley, J. S. Speagle, J. GroÎ2schedl, D. P. Finkbeiner, A. Burkert, D. Khimey, and C. Swiggum, Star formation near the Sun is driven by expansion of the local bubble, Nature (London) **601**, 334 (2022).
[42] B. Wehmeyer, A. Y. López, B. Côté, M. K. Pető, C. Kobayashi, and M. Lugaro, Inhomogeneous enrichment of radioactive nuclei in the galaxy: Deposition of live ^{53}Mn, ^{60}Fe, ^{182}Hf, and ^{244}Pu into deep-sea archives. Surfing the wave?, Astrophys. J. **944**, 121 (2023).